

SIGNAL PRESERVING WEIGHT INITIALIZATION FOR ODD-SIGMOID ACTIVATIONS

Hyunwoo Lee¹, Hayoung Choi^{2*}, Hyunju Kim^{3*}

¹Korea Institute for Advanced Study, ²Kyungpook National University,

³Korea Institute of Energy Technology

¹hyunwoolee@kias.re.kr, ²hayoung.choi@knu.ac.kr,

³hjkim@kentech.ac.kr

ABSTRACT

Activation functions critically influence trainability and expressivity, and recent work has therefore explored a broad range of nonlinearities. However, activations and weight initialization are interdependent: without an appropriate initialization method, nonlinearities can cause saturation, variance collapse, and increased learning-rate sensitivity. We address this by defining an odd-sigmoid function class and, given any activation f in this class, proposing an initialization method tailored to f . The method selects a noise scale in closed form so that forward activations remain well dispersed up to a target layer, thereby avoiding collapse to zero or saturation. Empirically, the approach trains reliably without normalization layers, exhibits strong data efficiency, and enables learning for activations under which standard initialization methods (Xavier, He, Orthogonal) often do not converge reliably.

1 INTRODUCTION

Deep learning has advanced substantially across diverse domains (LeCun et al., 2015; He et al., 2016; Hwang et al., 2022). Nonlinearity is introduced through activation functions, and recent work has explored alternatives beyond classical choices to improve trainability, stability, and accuracy (e.g., GELU, Swish, Mish, SELU) (Hendrycks & Gimpel, 2016; Ramachandran et al., 2017; Misra, 2019; Klambauer et al., 2017; Bingham & Miikkulainen, 2023; Zhang et al., 2024). Activation and weight initialization are interdependent (He et al., 2015). The scale and shape of the nonlinearity determine signal and gradient propagation at depth; with an initializer that is not appropriate for the activation, networks can saturate or exhibit variance collapse even when the activation itself is reasonable. Therefore, rather than fixing an initializer and searching over activations, it is preferable to design an activation-aware initialization matched to the chosen activation. This approach enables systematic exploration of a broader set of activations while preserving well-conditioned forward and backward signal flow.

Motivated by this, we propose activation-aware initialization for feedforward neural network (FFNN). We first define the odd-sigmoid function class \mathcal{F} : continuously differentiable, odd, bounded, strictly increasing activations with strictly decreasing derivatives on $[0, \infty)$ (see Figure 1). Building on this structure, we propose an initialization method tailored to $f \in \mathcal{F}$ that preserves forward signal propagation to a target depth L . The proposed initialization is derived from the pitchfork behavior of $x \mapsto f(ax)$ and a simplified signal-propagation model for f . This leads to a closed-form choice of σ^* that keeps activation distributions well

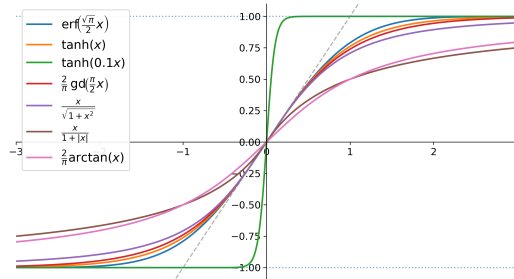


Figure 1: Odd-Sigmoid Activations

*Corresponding authors.

dispersed across layers, mitigating collapse to zero or saturation. Preserving such dispersion is important because network expressivity grows rapidly with depth (Poole et al., 2016; Raghu et al., 2017). We evaluate the proposed method on $f \in \mathcal{F}$ in two cases, with $\omega := 1/f'(0)$ either near 1 or far from 1, and compare against widely used initializations (Xavier (Glorot & Bengio, 2010), He (He et al., 2015), Orthogonal (Saxe et al., 2014)). Across a variety of f , our initializer is robust to learning-rate choice and yields faster early training and stronger data efficiency than the baselines; in particular, when ω is far from 1, the baselines often fail to learn while the proposed method remains trainable. In addition, the proposed initialization is robust across network sizes and reduces reliance on normalization layers such as Batch Normalization (BN) (Ioffe, 2015), thereby lowering the burden of hyperparameter tuning (e.g., depth/width selection) and avoiding the computational overhead associated with normalization. Our main contributions can be summarized as follows:

- We define the odd-sigmoid function class and, based on its properties, identify a condition relating the initialization, activation, and learning rate (Section 4.1 and 4.2).
- We propose a weight initialization for networks with odd-sigmoid activations that preserves and evenly propagates signal up to a target depth L (Section 4.2).
- We demonstrate that our method enables training even for activations that are typically difficult to optimize and achieves strong performance without batch normalization (Section 5).

2 RELATED WORK

Classic weight initialization methods stabilize layerwise variance; later work showed that good performance further hinges on tuning and momentum, such that first-order methods rival second-order only when initialization is well chosen, and surveys echo that improper statistics cause saturation, variance collapse, and learning-rate fragility (Sutskever et al., 2013; Narkhede et al., 2022). For sigmoidal nets, adjusting mean or support keeps units responsive (a small negative mean to avoid early gradient starvation, and mutual-information-based scale alignment), and spread-out mappings can speed convergence (Yilmaz & Poli, 2022; Qiao et al., 2016; Sodhi et al., 2014). Beyond first-order variance matching, curvature and correlation criteria matter: Hessian-norm control and depth \times width bounds inform safe step sizes, and propagation analyses under constraints (input-convex nets, transformers) show how choices prevent rank or gradient collapse (Skorski et al., 2021; Iyer et al., 2023; Hoedt & Klambauer, 2023; Noci et al., 2022). Architectural tweaks can also relieve fragile statistics (ReZero; dynamical-isometry-preserving setups for deep-narrow ReLU MLPs) (Bachlechner et al., 2021; Lee et al., 2024; Price et al., 2024; Blumenfeld et al., 2020). Overall, the literature argues for initialization calibrated to the activation and the network’s depth and shape, preserving variance and correlations through depth.

On the activation side, early bounded nonlinearities (Sigmoid, Tanh) suffered vanishing gradients, whereas ReLU variants improved efficiency but can produce dying neurons (Adeli et al., 2025). Surveys emphasize that no single activation is universally optimal and highlight desirable traits (continuity, boundedness, monotonicity, symmetry, smoothness) (Alcaide et al., 2025; Adeli et al., 2025), with bounded, odd-symmetric forms helping to center signals and stabilize optimization—directly motivating our initializer. Adaptive designs further reshape nonlinearities during training: scalable parametric activations improve convergence in DL and PINNs (Jagtap et al., 2020; Wang et al., 2023), and families such as AHerfReLU, ErfReLU, and Smish mitigate gradient or symmetry issues via analytic/error-function corrections (Ullah et al., 2025). Beyond globally shared forms, per-neuron self-activating networks learn piecewise-linear activations and boost accuracy on MNIST/CIFAR-10 (Tutuncuoglu, 2025), while zeroing neural networks employ tailored activations for finite-time convergence and robustness in matrix decomposition (Liu, 2025). Collectively, these results support initialization strategies aligned with activation structure—precisely the principle pursued here.

3 PRELIMINARY

In this section, we introduce the notation used throughout the paper and present a simplified analysis of signal propagation (Lee et al., 2025) in feedforward networks.

Notations. We consider a feedforward neural network with L layers. The dataset comprises K pairs $\{(\mathbf{x}_i, \mathbf{y}_i)\}_{i=1}^K$, where $\mathbf{x}_i \in \mathbb{R}^{N_x}$ is the input and $\mathbf{y}_i \in \mathbb{R}^{N_y}$ is the corresponding target. For $\ell = 1, \dots, L$, the layerwise update is

$$\mathbf{x}^\ell = f(\mathbf{W}^\ell \mathbf{x}^{\ell-1} + \mathbf{b}^\ell) \in \mathbb{R}^{N_\ell},$$

where $\mathbf{W}^\ell \in \mathbb{R}^{N_\ell \times N_{\ell-1}}$ is the weight matrix, $\mathbf{b}^\ell \in \mathbb{R}^{N_\ell}$ is the bias vector, and $f(\cdot)$ denotes an activation function. We write $\mathbf{W}^\ell = [w_{ij}^\ell]$.

Signal Propagation Analysis. Following the simplified framework of Lee et al. (2025), we analyze signal propagation in feedforward networks with an element-wise activation f . For convenience, all layers, including input and output, are assumed to have dimension n (i.e., $N_\ell = n$ for all ℓ). A key observation of this approach is that the usual matrix–vector multiplication $\mathbf{W}^\ell \mathbf{x}^{\ell-1}$ can be reformulated element-wise, so that each coordinate is expressed in terms of an effective self-scaling factor. Formally, for $\ell = 0, \dots, L-1$ and $i = 1, \dots, n$,

$$x_i^{\ell+1} = f(a_i^{\ell+1} x_i^\ell), \quad a_i^{\ell+1} = w_{ii}^{\ell+1} + \sum_{j \neq i} \frac{w_{ij}^{\ell+1} x_j^\ell}{x_i^\ell}, \quad (1)$$

assuming that $\mathbf{b}^\ell = \mathbf{0}$. This element-wise decomposition highlights the role of $a_i^{\ell+1}$ as an effective gain, combining both diagonal and off-diagonal terms, and provides a tractable basis for studying signal propagation in deep networks.

4 METHODOLOGY

We first define the odd–sigmoid function class (Section 4.1). Building on this, we propose a weight initialization for feedforward networks with odd–sigmoid activations (Section 4.2). The proofs of theoretical results are provided in Appendix A.

4.1 ODD-SIGMOID FUNCTION CLASS

In networks with sigmoidal activations, forward signals can saturate as depth increases, converging either to zero or to the activation’s extreme values. We address this by defining the odd–sigmoid function class (Figure 1). This class includes many well-known activations, such as $\tanh(x)$, $\arctan(x)$, $\text{softsign}_1(x)$, and $\text{erf}(x)$. Formal definitions of the activation functions used in this paper are provided in Appendix B.1.

Definition 4.1. A function $f : \mathbb{R} \rightarrow \mathbb{R}$ is an *Odd-Sigmoid Function* if it satisfies the following:

- (i) **Regularity:** $f \in C^1(\mathbb{R})$.
- (ii) **Odd symmetry:** $f(-x) = -f(x)$ for all $x \in \mathbb{R}$.
- (iii) **Boundedness:** $\sup_{x \in \mathbb{R}} |f(x)| < \infty$.
- (iv) **Strict monotonicity:** $f'(x) > 0$ for all $x \in \mathbb{R}$.
- (v) **Slope decay:** f' is strictly decreasing on $[0, \infty)$.

Denote the class of all odd-sigmoid functions as \mathcal{F} .

Pitchfork Bifurcation. Recall that $x^* \in \mathbb{R}$ is a fixed point of $f : \mathbb{R} \rightarrow \mathbb{R}$ if $f(x^*) = x^*$. For $f \in \mathcal{F}$ define $\omega_f := 1/f'(0) > 0$ and, unless stated otherwise, write ω simply. Consider $\phi_a(x) := f(ax)$ for $a > 0$. We say that ϕ_a has a pitchfork bifurcation at $a = \omega$ if it has exactly one fixed point $\{0\}$ for $0 < a < \omega$ and exactly three fixed points $\{0, \pm \xi_a\}$ for $a > \omega$, with the nonzero points occurring as a symmetric pair; we will show that this holds for every $f \in \mathcal{F}$.

Proposition 4.2. Suppose $f \in \mathcal{F}$ with $\omega := 1/f'(0)$, and for a fixed $a > 0$ define $\phi_a(x) := f(ax)$. Then

- (i) If $0 < a \leq \omega$, then $\phi_a(x)$ has a unique fixed point $x^* = 0$.

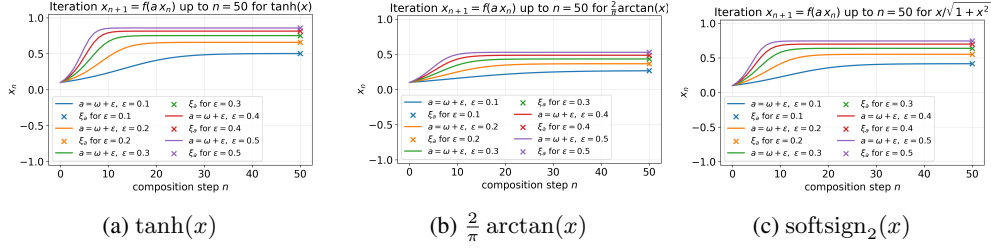


Figure 2: Convergence of the iteration $x_{n+1} = f(ax_n)$ for odd-sigmoid f with $a = \omega + \epsilon$ ($\epsilon \in \{0.1, 0.2, 0.3, 0.4, 0.5\}$); curves show x_n up to $n = 50$ from $x_0 = 0.1$, and ‘x’ marks the positive fixed point ξ_a solving $f(a\xi_a) = \xi_a$.

(ii) If $a > \omega$, then $\phi_a(x)$ has three distinct fixed points: $x^* = -\xi_a, 0, \xi_a$ such that $\xi_a > 0$.

The following theorem establishes convergence properties of $x_{n+1} = f(ax_n)$ for all $x_0 > 0$.

Theorem 4.3. Suppose $f \in \mathcal{F}$ with $\omega := 1/f'(0)$, and for a fixed $a > 0$ define

$$x_0 > 0, \quad x_{n+1} = \phi_a(x_n), \quad n = 0, 1, 2, \dots$$

Then the sequence $\{x_n\}$ converges for every $x_0 > 0$. Furthermore,

- (1) if $0 < a \leq \omega$, then $x_n \rightarrow 0$ as $n \rightarrow \infty$.
- (2) if $a > \omega$, then $x_n \rightarrow \xi_a$ as $n \rightarrow \infty$.

According to Theorem 4.3, when $a > \omega$, for any initial value $x_0 > 0$ (resp. $x_0 < 0$), the sequence defined by $x_{n+1} = f(ax_n)$ converges to ξ_a (resp. $-\xi_a$) as $n \rightarrow \infty$. From a signal-propagation viewpoint in FFNN (Equation 1), this implies that activations do not vanish as depth increases. See Figures. 2, 3 and 7 for the convergence of the iterates $x_{n+1} = \phi_a(x_n)$ as a function of a and the initial value x_0 . Proposition A.2 and Corollary A.3 analyze the iteration with a coefficient sequence $\{a_m\}$ that may vary across steps. They show that excessively large or small a_m drives the dynamics into saturation, highlighting the importance of appropriately scaling $\{a_m\}$ when designing the initialization.

Corollary 4.4. Let $f_1, f_2 \in \mathcal{F}$ and let $c_1, c_2 \geq 0$ with $(c_1, c_2) \neq (0, 0)$. If $g = c_1 f_1 + c_2 f_2$, then $g \in \mathcal{F}$. Furthermore, it holds that

$$\frac{1}{\omega_g} = \frac{c_1}{\omega_{f_1}} + \frac{c_2}{\omega_{f_2}}.$$

Since \mathcal{F} is closed under addition, more generally, any finite sum $\sum_{j=1}^M c_j f_j \in \mathcal{F}$ for all $c_j \geq 0$ with $(c_1, \dots, c_M) \neq \mathbf{0}$ and $f_j \in \mathcal{F}$.

4.2 PROPOSED WEIGHT INITIALIZATION METHOD

We propose a weight initialization method for odd-sigmoid activations that, in the initial forward pass, ensures the activation distribution is well dispersed across layers and avoids concentration near zero or saturation.

Proposed Weight Initialization. Consider $f \in \mathcal{F}$ with $\omega := 1/f'(0) > 0$ and a target depth L . We initialize each layer as $\mathbf{W}^\ell = \mathbf{D}^\ell + \mathbf{Z}^\ell \in \mathbb{R}^{N_\ell \times N_{\ell-1}}$, where $(\mathbf{D}^\ell)_{ij} = \omega$ if $i \equiv j \pmod{N_{\ell-1}}$ and 0 otherwise, and draw i.i.d. noise

$$(\mathbf{Z}^\ell)_{ij} \sim \mathcal{N}\left(0, (\sigma^*)^2/N_{\ell-1}\right).$$

σ^* is chosen for a target negative rate $p \in [0, \frac{1}{2})$ at depth L via

$$\sigma^*(p, L, \omega) = -\frac{\omega}{\Phi^{-1}\left(\frac{1 - (1 - 2p)^{1/L}}{2}\right)},$$

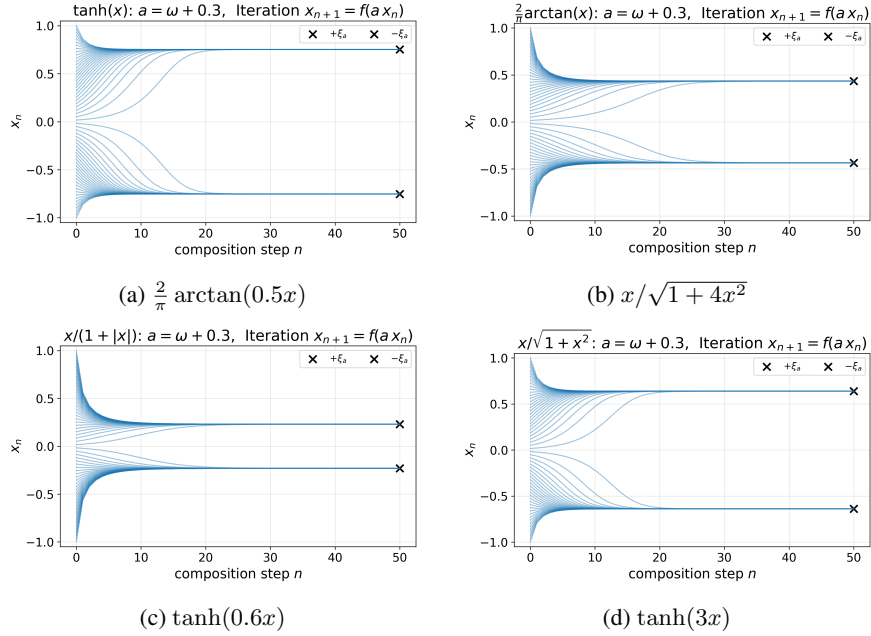


Figure 3: For each activation f , we iterate $x_{n+1} = f(ax_n)$ with $a = \omega + 0.3$ and $\omega = 1/f'(0)$ from 60 initial values $x_0 \in [-1, 1]$ up to $n = 50$; trajectories are shown (thin lines), and the fixed points $\pm\xi_a$ satisfying $f(a\xi_a) = \xi_a$ are marked at $n = 50$ with ‘x’.

where Φ denotes the standard normal cumulative distribution function (CDF). For the learning rate, we use a band proportional to ω ; for Adam (Kingma & Ba, 2014),

$$\eta \in [10^{-5}\omega, 10^{-3}\omega].$$

We discuss σ^* in Theorem 4.7 and the learning rate η in Table 3.

Lemma 4.5. *Using the elementwise formulation in equation 1 and employing the proposed weight initialization, fix an arbitrary layer ℓ and index i such that $x_i^\ell \neq 0$. Then, conditionally on x^ℓ ,*

$$a_i^{\ell+1} \sim \mathcal{N}\left(\omega, \frac{\sigma_z^2}{N_\ell} \left(1 + \sum_{j \neq i} \left(\frac{x_j^\ell}{x_i^\ell}\right)^2\right)\right),$$

and $\text{Var}(a_i^{\ell+1}) \geq \sigma_z^2/N_\ell$.

According to Lemma 4.5, $a_i^{\ell+1}$ is Gaussian with $\text{Var}(a_i^{\ell+1}) \geq \sigma_z^2/N_\ell$. In what follows, we do not model the exact law of $a_i^{\ell+1}$; for analytical convenience, we use the lower-bound variance σ_z^2/N_ℓ as a conservative surrogate.

Theorem 4.6. *Let $f \in \mathcal{F}$ and $N_\ell = 1$. Fix $x_0 > 0$ and an integer $m \geq 1$. Let a_1, \dots, a_m be i.i.d. Gaussian gains with distribution $\mathcal{N}(\omega, \sigma^2)$, and define*

$$a_{\min} := \min\{a_1, \dots, a_m\}, \quad \phi_a(x) := f(ax), \quad \Phi_m := \phi_{a_1} \circ \dots \circ \phi_{a_m} \quad \Phi_m^\alpha := \phi_\alpha \circ \dots \circ \phi_\alpha.$$

Then the following holds.

(i)

$$\Phi_m(x_0) \geq \underbrace{\phi_{a_{\min}} \circ \dots \circ \phi_{a_{\min}}}_{m \text{ times}}(x_0).$$

(ii) *For $\alpha > \omega > 0$, $\Phi_m^\alpha(x_0) \rightarrow \xi_\alpha$ where $\xi_\alpha > 0$. Hence for any $0 < x_0 < \delta < \xi_\alpha$ there exists $r \in \mathbb{N}$ with $\Phi_r^\alpha(x_0) \geq \delta$, and for all $m \geq r$,*

$$\mathbb{P}(\Phi_m(x_0) \geq \delta) \geq \left(1 - \Phi\left(\frac{\alpha - \omega}{\sigma}\right)\right)^r.$$

where Φ is the standard normal CDF.

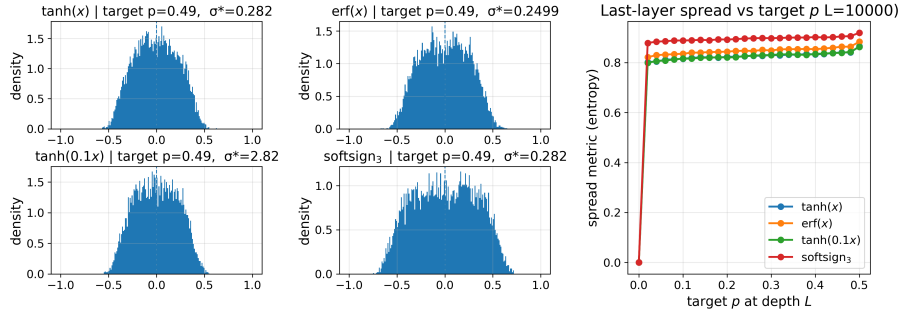


Figure 4: **(Left)** last-layer activation histograms at target $p = 0.3$ for four odd-sigmoid activations (\tanh , erf , $\tanh(0.1x)$, and softsign_3) in a depth-10,000 feedforward chain (width proxy $n = 20,000$, $x_0 > 0$). For each activation, the noise scale σ^* is set by the closed form $\pi_L(\sigma^*) = p$. **(Right)** last layer spread metric versus target p .

By Lemma 4.5, Theorem 4.6 applies directly to the actual FFNN forward propagation. This explains why, unlike zero-mean Gaussian initializations (e.g., Xavier/He) (Schoenholz et al., 2016), our method prevents the deep-layer activation distribution from collapsing to zero; see Figures 4, 9 and 10 for empirical evidence.

Negative Rate. We adopt the negative rate as an auxiliary statistic linking the surrogate dynamics to the FFNN. In the scalar surrogate, $\pi_L(\sigma)$ is strictly increasing in σ and attains $1/2$ only as $\sigma \rightarrow \infty$; hence for any target $p \in [0, \frac{1}{2})$ there exists a *unique* noise scale σ^* satisfying $\pi_L(\sigma^*) = p$ (invertible, closed form calibration). Moreover, by Lemma 4.5 the actual FFNN obeys $\text{Var}(a_i^{\ell+1}) \geq \sigma_z^2/N_\ell$, so the surrogate’s calibrated spread is not under-delivered at depth L . The calibration is well-conditioned on the practical range $p \in [0.30, 0.49]$, where $\pi_L(\sigma)$ has an appreciable slope while remaining far from its saturation at $1/2$. Accordingly, we choose p in this interval, compute σ^* , and verify the resulting scales in the full network. As shown in Figure 8, the empirical negative rate closely matches theory, and even at depth $L = 10^4$ the layer- L activation histograms for four odd-sigmoid activations remain broadly dispersed (see also Figure 9 and 10).

Theorem 4.7. Fix a target $p \in [0, \frac{1}{2})$, a depth $\ell \in \mathbb{N}$, and $\omega > 0$. There exists a unique $\sigma^* = \sigma^*(p, \ell, k) > 0$ such that $\pi_\ell(\sigma^*) = p$, and it is given by

$$\sigma^*(p, \ell, k) = - \frac{k}{\Phi^{-1}\left(\frac{1 - (1 - 2p)^{1/\ell}}{2}\right)}. \quad (2)$$

To summarize how well the last-layer distribution is dispersed as the target negative rate p varies, we employ a normalized histogram-entropy score

$$\text{Spread}(x) = \frac{-\sum_{i=1}^B p_i \log p_i}{\log B}, \quad p_i = \int_{\text{bin } i} \hat{f}_x(t) dt, \quad \sum_{i=1}^B p_i = 1,$$

where \hat{f}_x is the empirical density over $[-1, 1]$ using B bins. Values closer to 1 indicate a more dispersed (near-uniform) last layer distribution, while values near 0 indicate a concentrated distribution. Using this metric, we assess how the last layer spread changes with the target negative rate p .

5 EXPERIMENTS

In this section, we evaluate the proposed initialization. Section 5.1 assesses widely used activations with $\omega \approx 1$ on standard classification benchmarks, comparing our method with baseline initializations (e.g., Xavier, He, Orthogonal). Section 5.2 investigates activations with $\omega \not\approx 1$, focusing on performance, batch normalization effects, and learning-rate sensitivity.

Table 1: Average validation accuracy over 5 epochs for a 20-layer MLP (512 units) on MNIST and Fashion MNIST, comparing four initializations (Proposed, Xavier, He, Orthogonal). Columns correspond to odd-sigmoid activations $f \in \mathcal{F}$.

Dataset	Method	$\tanh(x)$	$\operatorname{erf}(x)$	$\arctan(x)$	$\operatorname{gd}(x)$	$\operatorname{softsign}_3(x)$	$\operatorname{softsign}_{1+3}(x)$
MNIST	Xavier	94.98	96.12	94.90	94.98	95.61	95.62
	He	96.32	96.03	96.33	96.60	96.55	89.17
	Orthogonal	95.21	96.48	95.21	94.93	95.71	95.60
	Proposed	96.88	97.00	96.87	96.84	96.94	95.51
FMNIST	Xavier	85.35	86.17	85.31	80.24	85.66	85.81
	He	86.92	86.82	86.98	80.59	86.78	81.48
	Orthogonal	85.99	87.10	85.70	83.01	86.00	86.48
	Proposed	87.01	87.16	87.20	83.39	86.11	86.21

Experimental Setting. We evaluate the proposed initialization on MNIST and Fashion-MNIST (FMNIST) using the Adam optimizer. Unless stated otherwise, we use a batch size of 128 and allocate 15% of the training data for validation. All experiments are implemented in TensorFlow without skip connections and without learning-rate decay. Unless otherwise noted, we set the target negative rate to $p = 0.30$ to calibrate σ^* , and we compare four initializations: Proposed, Xavier, He, and Orthogonal. The latter three are included because they are among the most widely used initialization schemes in practice.

5.1 EXPERIMENTS WITH $\omega \approx 1$ ACTIVATIONS

For each activation, with $\omega := 1/f'(0)$, we obtain $\tanh(x) : \omega = 1$; $\operatorname{erf}(x) : \omega = \sqrt{\pi}/2 \approx 0.886$; $\arctan(x) : \omega = 1$; $\operatorname{gd}(x) : \omega = 1$; $\operatorname{softsign}_3(x) : \omega = 1$; $\operatorname{softsign}_1(x) + \operatorname{softsign}_2(x) : \omega = 1/2$. Except for the composite $\operatorname{softsign}_1 + \operatorname{softsign}_2$ (and, to a lesser extent, erf), these ω values are near 1.

Early Epoch Performance. Table 1 reports average validation accuracy over 5 epochs for a 20-layer MLP (512 units) on MNIST and Fashion-MNIST, comparing four initializations (Proposed, Xavier, He, Orthogonal) across odd-sigmoid activations $f \in \mathcal{F}$. The proposed initialization attains the best accuracy in 9 of 12 settings (5/6 on MNIST and 4/6 on FMNIST), consistently outperforming the baselines for \tanh , erf , \arctan , and gd . On composite $\operatorname{softsign}_{1+3}$ (MNIST, FMNIST) and on $\operatorname{softsign}_3$ (FMNIST), a baseline slightly leads. Notably, \tanh is not the only viable choice of activation. Across datasets, the activation with the highest average accuracy is not always \tanh ; other odd-sigmoid functions sometimes attain the top result. We caution, however, that this observation is based on a limited set of tasks and epochs. Detailed experimental results are provided in Figure 11 and 12.

Dataset Efficiency. Table 2 presents the best validation accuracy within 10 epochs for a 20-layer FFNN (512 units) on MNIST and FMNIST, trained on small subsets of size 100 or 500. We compare four initializations across odd-sigmoid activations $f \in \mathcal{F}$. The proposed initialization attains the top accuracy in all settings—across both datasets and both sample regimes—with the gains most pronounced at 100 samples. These results indicate that our method is data-efficient, achieving higher validation accuracy with limited data and a small number of training epochs. Detailed experimental results are provided in Figure 13 and 14.

5.2 EXPERIMENTS WITH ACTIVATIONS FAR FROM $\omega \approx 1$

For

$$f(x) = \tanh(ax) + \operatorname{erf}(bx) + \frac{x}{1 + |cx|} + \operatorname{gd}(dx), \quad (3)$$

by Corollary 4.4 this f is an odd-sigmoid activation $\omega = 1/(a + \frac{2}{\sqrt{\pi}}b + c + d)$. Empirical results for various (a, b, c, d) appear in Figure 5. This section focuses on activations with ω far from 1.

Batch Normalization Free Training. Figure 5 evaluates a 100 layer MLP (64 units) on MNIST with a 1,000-sample subset using the composite odd-sigmoid activation $f(x) = \tanh(ax) +$

Table 2: Best validation accuracy within 10 epochs for a 20-layer FFNN (512 units) on MNIST and FMNIST, trained on 100 or 500 sample subsets, comparing initializations (Xavier, He, Orthogonal, Proposed) across odd-sigmoid activations.

Dataset	Method	tanh(x)		erf(x)		arctan(x)		gd(x)		softsign ₃ (x)		softsign ₁ (x) + softsign ₂ (x)	
		100	500	100	500	100	500	100	500	100	500	100	500
MNIST	Xavier	61.45	84.05	60.40	85.45	60.13	83.90	59.93	84.77	61.52	84.48	43.90	76.83
	He	54.40	84.60	60.46	76.67	56.62	84.68	57.60	83.48	51.35	84.00	22.63	40.13
	Orthogonal	62.92	86.47	64.58	86.75	62.97	85.87	62.70	86.38	62.35	86.22	47.62	80.58
	Proposed	64.60	86.93	64.97	87.00	63.23	86.88	64.23	86.62	62.77	87.13	63.62	85.77
FMNIST	Xavier	58.13	76.78	67.02	76.78	64.35	77.12	60.55	76.30	63.00	75.02	58.40	75.72
	He	66.08	78.38	58.80	74.63	66.28	76.40	63.15	78.30	65.33	76.87	26.00	57.28
	Orthogonal	64.40	78.90	67.57	78.58	63.45	78.32	64.35	78.10	66.40	78.37	68.30	77.20
	Proposed	69.00	79.25	70.13	79.07	70.73	78.40	70.03	78.92	70.32	78.87	67.93	78.23

$\text{erf}(bx) + x/(1 + |cx|) + \text{gd}(dx)$ under three coefficient settings (a) (1, 1, 1, 1), (b) (3, 4, 2, 0.1), and (c) (300, 300, 200, 500), each yielding $\omega = 1/f'(0)$ far from 1. Across all settings, the proposed initialization achieves the highest validation accuracy and maintains non-vanishing signal propagation to deep layers, despite limited data and without relying on batch normalization. Baselines and their +BN variants fail to match this performance, highlighting that the proposed scheme enables stable, BN-free training even when ω is far from the near-critical regime.

Learnable Learning Rate. Table 3 presents the learnable learning-rate ranges activation function-ter one epoch for a 20-layer MLP (512 units) on MNIST, trained on a 1,000-sample subset. Rows compare four initializations across three odd-sigmoid activations $f(\alpha x)$ with scale α . We evaluate only a single epoch to rapidly probe initial learnability. The proposed method consistently yields a learnable, typically wider LR window across a broad range of α , demonstrating that training remains feasible across diverse ω -scales. Detailed experimental results are provided in Figure 15, 16 and 6.

Our approach sets the noise level by $\sigma^* = \sigma^*(p, L, \omega)$. If the learning rate is chosen far above or below an ω -scaled band, the first parameter update tends to destroy the calibrated noise spread, collapsing the forward statistics from the second pass onward. Motivated by this, we adopt the practical LR range

$$\eta \in [10^{-5} \omega, 10^{-3} \omega].$$

6 CONCLUSION

We proposed an initialization method that adapts to activations drawn from the odd-sigmoid family and demonstrated that a simple, activation-aware calibration of the noise scale at a target depth can substantially improve early trainability. Empirically, the approach is data-efficient, robust to depth and width, and trains reliably without normalization layers; on commonly used activations it consistently outperforms standard methods (Xavier, He, Orthogonal) in the initial learning phase.

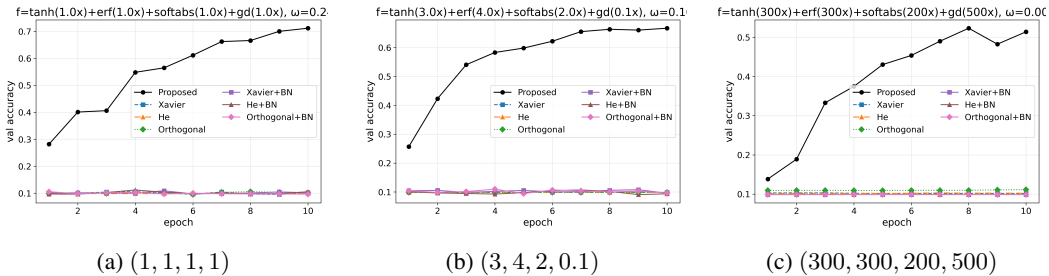


Figure 5: Validation accuracy over 10 epochs for a 100 layer MLP (64 units) on MNIST, trained on a 1,000-sample subset with Adam. Seven initializations are compared: Proposed, Xavier, He, Orthogonal, and their +BN variants. The activation is $f(x) = \tanh(ax) + \text{erf}(bx) + x/(1 + |cx|) + \text{gd}(dx)$ with coefficients shown in (a) (1, 1, 1, 1), (b) (3, 4, 2, 0.1), and (c) (300, 300, 200, 500) (the corresponding $\omega = 1/f'(0)$ appears in each title).

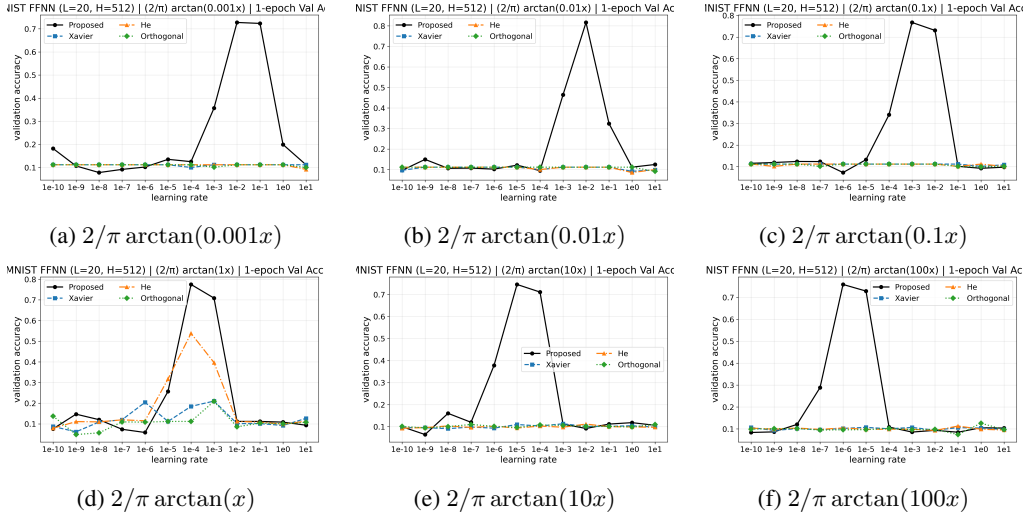


Figure 6: Learnable learning rate ranges activation functionter one epoch for a 20-layer MLP (width 512) on MNIST, trained on a 1,000-sample subset. Panels report one-epoch validation accuracy for $f(x) = 2/\pi \arctan(\alpha x)$ with $\alpha \in \{10^{-3}, 10^{-2}, 10^{-1}, 1, 10, 100\}$ across four initializations (Proposed, Xavier, He, Orthogonal).

Because it does not rely on Batch Normalization and remains stable across depths/widths, it reduces the memory overhead of normalization layers and also lowers the amount of depth/width tuning required, yielding tangible computational savings in practice. By explicitly targeting a well-spread activation distribution at a specified depth in the first forward pass, the method preserves stable signal propagation and reduces the incidence of saturation or variance collapse—two primary failure modes of depth.

The procedure improves the conditions for effective training but does not guarantee convergence in every setting, and our theoretical calibration is derived for odd-sigmoids with a depthwise surrogate model. Extending the analysis to broader activation classes, residual and convolutional architectures, and diverse objectives is a promising direction. Further, exploring adaptive or per-layer schedules for σ , and combining the initialization with light-weight normalization or curriculum strategies, may yield additional gains. Overall, the evidence indicates that activation-aware initialization is a practical mechanism for broadening the activation design space while maintaining stable signal propagation and strong early learning performance.

Table 3: Learnable learning-rate ranges activation functionter 1 epoch for a 20-layer MLP (width 512) on MNIST, trained on a 1,000-sample subset. Rows compare four initializations (Xavier, He, Orthogonal, Proposed) across three odd-sigmoid activations ($\tanh(\alpha x)$, $\operatorname{erf}(\alpha x)$, and $(2/\pi) \arctan(\alpha x)$). “—” indicates that the model failed to train under all tested learning rates.

Dataset	Method	$\alpha = 1000$	100	10	1	0.1	0.01	0.001
$\tanh(\alpha x)$	Xavier	—	—	—	$10^{-5}\text{--}10^{-3}$	—	—	—
	He	—	—	—	$10^{-5}\text{--}10^{-4}$	—	—	—
	Orthogonal	—	—	—	$10^{-5}\text{--}10^{-3}$	—	—	—
	Proposed	$10^{-8}\text{--}10^{-6}$	$10^{-7}\text{--}10^{-5}$	$10^{-6}\text{--}10^{-4}$	$10^{-5}\text{--}10^{-3}$	$10^{-4}\text{--}10^{-2}$	$10^{-3}\text{--}10^{-2}$	$10^{-3}\text{--}10^{-1}$
$\operatorname{erf}(\alpha x)$	Xavier	—	—	—	$10^{-5}\text{--}10^{-4}$	—	—	—
	He	—	—	—	$10^{-5}\text{--}10^{-4}$	—	—	—
	Orthogonal	—	—	—	$10^{-5}\text{--}10^{-3}$	—	—	—
	Proposed	$10^{-9}\text{--}10^{-6}$	$10^{-7}\text{--}10^{-5}$	$10^{-7}\text{--}10^{-4}$	$10^{-5}\text{--}10^{-3}$	$10^{-4}\text{--}10^{-2}$	$10^{-3}\text{--}10^{-2}$	$10^{-3}\text{--}10^{-1}$
$2/\pi \arctan(\alpha x)$	Xavier	—	—	—	$10^{-4}\text{--}10^{-3}$	—	—	—
	He	—	—	—	$10^{-5}\text{--}10^{-3}$	—	—	—
	Orthogonal	—	—	—	10^{-3}	—	—	—
	Proposed	$10^{-9}\text{--}10^{-6}$	$10^{-7}\text{--}10^{-5}$	$10^{-6}\text{--}10^{-4}$	$10^{-5}\text{--}10^{-3}$	$10^{-4}\text{--}10^{-2}$	$10^{-3}\text{--}10^{-1}$	$10^{-3}\text{--}10^0$

REFERENCES

- Behtom Adeli, John P. McLinden, Pankaj Pandey, Ming Shao, and Yalda Shahriari. Toward improving fnirs classification: A study on activation functions in deep neural architectures. *arXiv preprint*, 2025.
- Daniel Alcaide, Marta Gonzalez, Juan Ramirez, and Luis Ortega. Telu activation function for fast and stable deep learning. *Information Sciences*, 690:120345, 2025.
- Thomas Bachlechner, Bodhisattwa Prasad Majumder, Henry Mao, Gary Cottrell, and Julian McAuley. Rezero is all you need: Fast convergence at large depth. In *Proceedings of the Thirty-Seventh Conference on Uncertainty in Artificial Intelligence (UAI 2021)*, pp. 1352–1361. PMLR, 2021.
- Garrett Bingham and Risto Miikkulainen. Efficient activation function optimization through surrogate modeling. *Advances in Neural Information Processing Systems*, 36:6634–6661, 2023.
- Yaniv Blumenfeld, Dar Gilboa, and Daniel Soudry. Beyond signal propagation: Is feature diversity necessary in deep neural network initialization? In *Proceedings of the 37th International Conference on Machine Learning*, pp. PMLR 119, 2020. PMLR, 2020.
- Xavier Glorot and Yoshua Bengio. Understanding the difficulty of training deep feedforward neural networks. In *International Conference on Artificial Intelligence and Statistics*, pp. 249–256, 2010.
- Kaiming He, Xiangyu Zhang, Shaoqing Ren, and Jian Sun. Delving deep into rectifiers: Surpassing human-level performance on imagenet classification. In *Proceedings of the IEEE International Conference on Computer Vision*, pp. 1026–1034, 2015.
- Kaiming He, Xiangyu Zhang, Shaoqing Ren, and Jian Sun. Deep residual learning for image recognition. In *Proceedings of the IEEE Conference on Computer Vision and Pattern Recognition*, pp. 770–778, 2016.
- Dan Hendrycks and Kevin Gimpel. Gaussian error linear units (gelus). *arXiv preprint arXiv:1606.08415*, 2016.
- Pieter-Jan Hoedt and G’unter Klambauer. Principled weight initialisation for input-convex neural networks. In *37th Conference on Neural Information Processing Systems (NeurIPS 2023)*, 2023.
- Jiyoung Hwang, Byeongjoon Noh, Zhixiong Jin, and Hwasoo Yeo. Asymmetric long-term graph multi-attention network for traffic speed prediction. In *2022 IEEE 25th International Conference on Intelligent Transportation Systems (ITSC)*, pp. 1498–1503. IEEE, 2022.
- Sergey Ioffe. Batch normalization: Accelerating deep network training by reducing internal covariate shift. *arXiv preprint arXiv:1502.03167*, 2015.
- Gaurav Iyer, Boris Hanin, and David Rolnick. Maximal initial learning rates in deep relu networks. In *Proceedings of the 40th International Conference on Machine Learning*, pp. 1–30. PMLR, 2023.
- Ameya D. Jagtap, Kenji Kawaguchi, and George Em Karniadakis. Adaptive activation functions accelerate convergence in deep and physics-informed neural networks. *Journal of Computational Physics*, 404:109136, 2020.
- Diederik P Kingma and Jimmy Ba. Adam: A method for stochastic optimization. *arXiv preprint arXiv:1412.6980*, 2014.
- G’unter Klambauer, Thomas Unterthiner, Andreas Mayr, and Sepp Hochreiter. Self-normalizing neural networks. *Advances in neural information processing systems*, 30, 2017.
- Yann LeCun, Yoshua Bengio, and Geoffrey Hinton. Deep learning. *Nature*, 521(7553):436–444, 2015.
- Hyunwoo Lee, Yunho Kim, Seung Yeop Yang, and Hayoung Choi. Improved weight initialization for deep and narrow feedforward neural network. *arXiv preprint arXiv:2311.03733*, 2024.

-
- Hyunwoo Lee, Hayoung Choi, and Hyunju Kim. Robust weight initialization for tanh neural networks with fixed point analysis. In *The Thirteenth International Conference on Learning Representations*, 2025.
- Xun Liu. A novel zeroing neural network with activation function-enhanced convergence for efficient data matrix decomposition. *Neurocomputing*, 616:128391, 2025.
- Diganta Misra. Mish: A self regularized non-monotonic activation function. *arXiv preprint arXiv:1908.08681*, 2019.
- Meenal V. Narkhede, Prashant P. Bartakke, and Mukul S. Sutaone. A review on weight initialization strategies for neural networks. *Artificial Intelligence Review*, 55:291–322, 2022.
- Lorenzo Noci, Luca Biggio, Sotiris Anagnostidis, Antonio Orvieto, Sidak Pal Singh, and Aurelien Lucchi. Signal propagation in transformers: Theoretical perspectives and the role of rank collapse. In *36th Conference on Neural Information Processing Systems (NeurIPS 2022)*, 2022.
- Ben Poole, Subhaneil Lahiri, Maithra Raghu, Jascha Sohl-Dickstein, and Surya Ganguli. Exponential expressivity in deep neural networks through transient chaos. *Advances in neural information processing systems*, 29, 2016.
- Ilan Price, Nicholas Daultry Ball, Samuel C.H. Lam, Adam C. Jones, and Jared Tanner. Deep neural network initialization with sparsity inducing activations. *Published as a conference paper at ICLR 2024*, 2024.
- Junfei Qiao, Sanyi Li, and Wenjing Li. Mutual information based weight initialization method for sigmoidal feedforward neural networks. *Neurocomputing*, 207:676–683, 2016. doi: 10.1016/j.neucom.2016.05.054.
- Maithra Raghu, Ben Poole, Jon Kleinberg, Surya Ganguli, and Jascha Sohl-Dickstein. On the expressive power of deep neural networks. In *International Conference on Machine Learning*, pp. 2847–2854, 2017.
- Prajit Ramachandran, Barret Zoph, and Quoc V Le. Searching for activation functions. *arXiv preprint arXiv:1710.05941*, 2017.
- Andrew M Saxe, James McClelland, and Surya Ganguli. Exact solutions to the nonlinear dynamics of learning in deep linear neural networks. In *International Conference on Learning Representations*, 2014.
- Samuel S Schoenholz, Justin Gilmer, Surya Ganguli, and Jascha Sohl-Dickstein. Deep information propagation. *arXiv preprint arXiv:1611.01232*, 2016.
- Maciej Skorski, Alessandro Temperoni, and Martin Theobald. Revisiting weight initialization of deep neural networks. *Proceedings of Machine Learning Research*, 157, 2021.
- Sartaj Singh Sodhi, Pravin Chandra, and Sharad Tanwar. A new weight initialization method for sigmoidal feedforward artificial neural networks. In *2014 International Joint Conference on Neural Networks (IJCNN)*, pp. 291–298. IEEE, 2014.
- Ilya Sutskever, James Martens, George Dahl, and Geoffrey Hinton. On the importance of initialization and momentum in deep learning. In *Proceedings of the 30th International Conference on Machine Learning*, JMLR: W&CP volume 28, pp. –, Atlanta, Georgia, USA, 2013. JMLR.org.
- Bekir Tolga Tutuncuoglu. Neuron-level activation learning in neural networks: A self-configuring ai approach. *SSRN*, 2025.
- Abaid Ullah, Muhammad Imran, Muhammad Abdul Basit, Madeeha Tahir, and Jihad Younis. Aherfrelu: A novel adaptive activation function enhancing deep neural network performance. *Complexity*, 2025:8233876, 2025.
- Honghui Wang, Lu Lu, Shiji Song, and Gao Huang. Learning specialized activation functions for physics-informed neural networks. *arXiv preprint*, 2023.

Ahmet Yilmaz and Riccardo Poli. Successfully and efficiently training deep multi-layer perceptrons with logistic activation function simply requires initializing the weights with an appropriate negative mean. *Neural Networks*, 153:87 – 103, 2022. URL <https://doi.org/10.1016/j.neunet.2022.05.030>.

Shijun Zhang, Jianfeng Lu, and Hongkai Zhao. Deep network approximation: Beyond relu to diverse activation functions. *Journal of Machine Learning Research*, 25(35):1–39, 2024.

SUPPLEMENTARY MATERIAL

The supplementary material is structured as follows.

- Appendix A provides the theoretical results and their proofs.
- Appendix B contains additional simulation results without neural networks.
- Appendix C reports extra experimental details and results with neural networks.

A THEORETICAL RESULTS

In this section, we provide proofs for the statements presented in Section 4.

A.1 THEORETICAL RESULTS FOR SECTION 4.1

Lemma A.1. *If $f \in \mathcal{F}$, then the following holds.*

- (i) $f(0) = 0$.
- (ii) $0 = \arg \max |f'(x)|$.
- (iii) $\lim_{x \rightarrow \infty} f'(x) = 0$.

Proof. (i) It is trivial that odd symmetry implies $f(0) = 0$. (ii) Since f' is an even function, by Definition 4.1(v) $f'(x)$ has the maximum value at $x = 0$. (iii) Since f' is strictly decreasing on $[0, \infty)$ and $f'(x) > 0$ for all $x \in \mathbb{R}$, the Monotone Convergence Theorem for real functions implies that $\ell := \lim_{x \rightarrow \infty} f'(x)$ exists for some $\ell \in [0, \infty)$. Suppose that $\ell > 0$. Then there exists $R > 0$ such that

$$f'(x) \geq \frac{\ell}{2} \quad \text{for all } x \geq R.$$

Integrating from R to x , we obtain

$$f(x) - f(R) = \int_R^x f'(t) dt \geq \frac{\ell}{2}(x - R) \quad \text{for all } x > R.$$

Hence $f(x) \rightarrow \infty$ as $x \rightarrow \infty$, which contradicts the boundedness of f . Therefore $\ell = 0$. \square

Proposition 4.2 Suppose $f \in \mathcal{F}$ with $\omega := 1/f'(0)$, and for a fixed $a > 0$ define $\phi_a(x) := f(ax)$. Then

- (i) If $0 < a \leq \omega$, then $f(ax)$ has a unique fixed point $x^* = 0$.
- (ii) If $a > \omega$, then $f(ax)$ has three distinct fixed points: $x^* = -\xi_a, 0, \xi_a$ such that $\xi_a > 0$.

Proof. For $a > 0$, consider $g(x, a) := f(ax) - x$. We have $g(0, a) = 0$ and $g'(x, a) = a f'(ax) - 1$.

Case (i): $0 < a \leq \omega$. For $x > 0$ we have $ax > 0$, and $f'(ax) < f'(0)$; hence

$$g'(x, a) = a f'(ax) - 1 < a f'(0) - 1 \leq 0,$$

for all $x > 0$. Thus $g(\cdot, a)$ is strictly decreasing on $(0, \infty)$, $g(0, a) = 0$, and $\lim_{x \rightarrow \infty} g(x, a) = L - x = -\infty$, so $g(x, a) < 0$ for all $x > 0$ and there is no positive root. Since $g(\cdot, a)$ is odd, there is no negative root either. Hence $x = 0$ is the unique solution.

Case (ii): $a > \omega$. Then $g'(0, a) = a f'(0) - 1 > 0$. $g'(\cdot, a)$ is strictly decreasing on $[0, \infty)$, and by the Lemma A.1

$$\lim_{x \rightarrow \infty} g'(x, a) = a \lim_{x \rightarrow \infty} f'(ax) - 1 = -1 < 0.$$

By the intermediate value theorem, there exists a unique $\hat{x} > 0$ with $g'(\hat{x}, a) = 0$. Hence $g(\cdot, a)$ is strictly increasing on $[0, \hat{x}]$ and strictly decreasing on $[\hat{x}, \infty)$. Since $g(0, a) = 0$ and $g'(0, a) > 0$, we have $g(x, a) > 0$ for all $0 < x \leq \hat{x}$. Using (3), $\lim_{x \rightarrow \infty} g(x, a) = -\infty$; because g is strictly decreasing on $[\hat{x}, \infty)$ and continuous, there exists a unique $\xi_a > \hat{x}$ with $g(\xi_a, a) = 0$. Thus, there is exactly one positive, nonzero root. Oddness of g yields the symmetric negative root $-\xi_a$, so the full set of real solutions is $\{-\xi_a, 0, \xi_a\}$. \square

Theorem 4.3 Suppose $f \in \mathcal{F}$ with $\omega := 1/f'(0)$, and for a fixed $a > 0$ define

$$x_0 > 0, \quad x_{n+1} = \phi_a(x_n), \quad n = 0, 1, 2, \dots$$

Then the sequence $\{x_n\}$ converges for every $x_0 > 0$. Furthermore,

- (1) if $0 < a \leq \omega$, then $x_n \rightarrow 0$ as $n \rightarrow \infty$.
- (2) if $a > \omega$, then $x_n \rightarrow \xi_a$ as $n \rightarrow \infty$.

Proof. (1) Since f is odd and f' is strictly decreasing on $[0, \infty)$, we have $0 < f'(x) < f'(0)$ for all $x \neq 0$; hence, for any $a \in (0, \omega)$ and any $x_n > 0$, it follows that $x_{n+1} = f(ax_n) < x_n$ for all $n \in \mathbb{N}$. By the monotone convergence theorem, it converges to the fixed point $x^* = 0$.

(2) Let $x_0 < \xi_a$. Since $\phi'(x)$ is decreasing for $x \geq 0$, with ξ_a is the unique fixed point for $x > 0$, it holds that $x_n < x_{n+1} < \xi_a$ for all $n \in \mathbb{N}$. Thus, by the monotone convergence theorem, the sequence converges to the fixed point ξ_a . The proof is similar when $x_0 > \xi_a$. By the monotone convergence theorem, the sequence also converges to the fixed point ξ_a . \square

Corollary 4.4 Let $f_1, f_2 \in \mathcal{F}$ and let $c_1, c_2 \geq 0$ with $(c_1, c_2) \neq (0, 0)$. If $g = c_1 f_1 + c_2 f_2$, then $g \in \mathcal{F}$. Furthermore, it holds that

$$\frac{1}{\omega_g} = \frac{c_1}{\omega_{f_1}} + \frac{c_2}{\omega_{f_2}}.$$

Proof. Since $\alpha, \beta \geq 0$, the linear combination preserves all items in the definition of \mathcal{F} : oddness and bounded saturation by linearity; strict monotonicity because $h'(x) = \alpha f'(x) + \beta g'(x) > 0$; and slope decay on $[0, \infty)$ because a positive linear combination of strictly decreasing functions is strictly decreasing. Hence $h \in \mathcal{F}$, and evaluating at 0 yields $h'(0) = \alpha f'(0) + \beta g'(0)$ and the stated k_h . Applying the pitchfork bifurcation theorem to h gives the final claim. \square

A.2 THEORETICAL RESULTS FOR SECTION 4.2

Proposition A.2. Let $f \in \mathcal{F}$ and $\{a_n\}_{n=1}^\infty$ be a positive real sequence, i.e., $a_n > 0$ for all $n \in \mathbb{N}$, such that only finitely many elements are greater than $\omega = 1/f'(0)$. For a positive sequence $\{a_n\}_{n \geq 1}$, set

$$\Phi_m := \phi_{a_m} \circ \phi_{a_{m-1}} \circ \dots \circ \phi_{a_1}.$$

Then for any $x \in \mathbb{R}$

$$\lim_{m \rightarrow \infty} \Phi_m(x) = 0.$$

Proof. Let $N := \max\{n : a_n > \omega\}$ (take $N = 0$ if the set is empty) and define

$$b_n = \begin{cases} a_n, & n \leq N, \\ 0, & n > N, \end{cases} \quad c_n = \begin{cases} a_n, & n \leq N, \\ \omega, & n > N. \end{cases}$$

Let $\hat{\Phi}_m := \phi_{b_m} \circ \dots \circ \phi_{b_1}$ and $\tilde{\Phi}_m := \phi_{c_m} \circ \dots \circ \phi_{c_1}$. For $x \geq 0$ and $n > N$, by definition of \mathcal{F} , we obtain

$$\hat{\Phi}_m(x) \leq \Phi_m(x) \leq \tilde{\Phi}_m(x).$$

Oddness yields the same in absolute value for all $x \in \mathbb{R}$:

$$|\hat{\Phi}_m(x)| \leq |\Phi_m(x)| \leq |\tilde{\Phi}_m(x)|.$$

By Proposition 4.3, $\hat{\Phi}_m(x) \rightarrow 0$ and $\tilde{\Phi}_m(x) \rightarrow 0$. The squeeze theorem gives $\Phi_m(x) \rightarrow 0$. \square

Corollary A.3. Let $\epsilon > 0$ be given and set $\omega := 1/f'(0)$. Suppose that $\{a_n\}_{n=1}^\infty$ be a positive real sequence such that only finitely many elements are lower than $k + \epsilon$. Then for any $x \in \mathbb{R} \setminus \{0\}$

$$\liminf_{m \rightarrow \infty} |\Phi_m(x)| \geq \xi_{\omega+\epsilon}.$$

Proof. Let $N := \max\{n : a_n < \omega + \epsilon\}$ (take $N = 0$ if the set is empty) and define

$$b_n = \begin{cases} a_n, & n \leq N, \\ \omega + \epsilon, & n > N. \end{cases} \quad \hat{\Phi}_m := \phi_{b_m} \circ \cdots \circ \phi_{b_1}, \quad \Phi_m := \phi_{a_m} \circ \cdots \circ \phi_{a_1},$$

where $\phi_a(x) := f(ax)$. By definition of \mathcal{F} ,

$$|\hat{\Phi}_m(x)| \leq |\Phi_m(x)| \quad (\forall x \in \mathbb{R}, \forall m).$$

Taking \liminf in the inequality yields

$$\liminf_{m \rightarrow \infty} |\Phi_m(x)| \geq \xi_{\omega + \epsilon}.$$

□

Lemma 4.5 Under equation 1 and the *proposed weight initialization* stated above, fix any layer ℓ and index i with $x_i^\ell \neq 0$. Then, conditionally on x^ℓ ,

$$a_i^{\ell+1} \sim \mathcal{N}\left(\omega, \frac{\sigma_z^2}{N_\ell} \left(1 + \sum_{j \neq i} \left(\frac{x_j^\ell}{x_i^\ell}\right)^2\right)\right),$$

and $\text{Var}(a_i^{\ell+1}) \geq \sigma_z^2/N_\ell$.

Proof. From equation 1 and the initialization (the diagonal of $\mathbf{D}^{\ell+1}$ equals ω and $\mathbf{Z}^{\ell+1}$ has i.i.d. entries $\mathcal{N}(0, \sigma_z^2/N_\ell)$), the pre-activation at coordinate i reads

$$s_i^{\ell+1} = \sum_{j=1}^{N_\ell} ((\mathbf{D}^{\ell+1})_{ij} + (\mathbf{Z}^{\ell+1})_{ij}) x_j^\ell = \omega x_i^\ell + (\mathbf{Z}^{\ell+1})_{ii} x_i^\ell + \sum_{j \neq i} (\mathbf{Z}^{\ell+1})_{ij} x_j^\ell.$$

On the event $x_i^\ell \neq 0$,

$$a_i^{\ell+1} = \frac{s_i^{\ell+1}}{x_i^\ell} = \omega + (\mathbf{Z}^{\ell+1})_{ii} + \sum_{j \neq i} (\mathbf{Z}^{\ell+1})_{ij} \frac{x_j^\ell}{x_i^\ell}.$$

Conditioning on x^ℓ , the coefficients $\{x_j^\ell/x_i^\ell\}_{j \neq i}$ are deterministic, while $\{(\mathbf{Z}^{\ell+1})_{ij}\}_{j=1}^{N_\ell}$ are independent centered Gaussians with variance σ_z^2/N_ℓ . Hence $a_i^{\ell+1} | x^\ell$ is Gaussian with mean ω and

$$\text{Var}(a_i^{\ell+1} | x^\ell) = \frac{\sigma_z^2}{N_\ell} \left(1 + \sum_{j \neq i} \left(\frac{x_j^\ell}{x_i^\ell}\right)^2\right) \geq \frac{\sigma_z^2}{N_\ell}.$$

Finally,

$$\text{Var}(a_i^{\ell+1}) = \mathbb{E}[\text{Var}(a_i^{\ell+1} | x^\ell)] + \text{Var}(\mathbb{E}[a_i^{\ell+1} | x^\ell]) = \mathbb{E}[\text{Var}(a_i^{\ell+1} | x^\ell)] \geq \frac{\sigma_z^2}{N_\ell},$$

since $\mathbb{E}[a_i^{\ell+1} | x^\ell] = \omega$ is constant. □

Lemma A.4. Let $f \in \mathcal{F}$ and for $a > 0$ define $\phi_a(x) := f(ax)$. Fix $x_0 \geq 0$ and two sequences $\{a_j\}_{j=1}^m, \{b_j\}_{j=1}^m$ with $0 \leq a_j \leq b_j$ for all j . Then

$$\Phi_m^{(a)}(x_0) := \phi_{a_1} \circ \cdots \circ \phi_{a_m}(x_0) \leq \Phi_m^{(b)}(x_0) := \phi_{b_1} \circ \cdots \circ \phi_{b_m}(x_0).$$

Proof. Since f is increasing, for $x \geq 0$ we have (i) $x \leq y \Rightarrow \phi_a(x) \leq \phi_a(y)$ and (ii) $a \leq b \Rightarrow \phi_a(x) \leq \phi_b(x)$. With $x_j^{(a)} = \phi_{a_j}(x_{j-1}^{(a)})$, $x_j^{(b)} = \phi_{b_j}(x_{j-1}^{(b)})$, the induction step is

$$x_j^{(a)} \leq \phi_{a_j}(x_{j-1}^{(b)}) \leq \phi_{b_j}(x_{j-1}^{(b)}) = x_j^{(b)} \quad \text{whenever } x_{j-1}^{(a)} \leq x_{j-1}^{(b)}.$$

Hence $x_m^{(a)} \leq x_m^{(b)}$, i.e. $\Phi_m^{(a)}(x_0) \leq \Phi_m^{(b)}(x_0)$. □

Theorem 4.6 Let $f \in \mathcal{F}$ and $N_\ell = 1$. Fix $x_0 > 0$ and an integer $m \geq 1$. Let a_1, \dots, a_m be i.i.d. Gaussian gains with distribution $\mathcal{N}(\omega, \sigma^2)$, and define

$$a_{\min} := \min\{a_1, \dots, a_m\}, \quad \phi_a(x) := f(ax), \quad \Phi_m := \phi_{a_1} \circ \dots \circ \phi_{a_m} \quad \Phi_m^\alpha := \phi_\alpha \circ \dots \circ \phi_\alpha.$$

Then the following hold.

(i)

$$\Phi_m(x_0) \geq \underbrace{\phi_{a_{\min}} \circ \dots \circ \phi_{a_{\min}}}_{m \text{ times}}(x_0).$$

(ii) For $\alpha > \omega > 0$, $\Phi_m^\alpha(x_0) \rightarrow \xi_\alpha$ where $\xi_\alpha > 0$. Hence for any $0 < x_0 < \delta < \xi_\alpha$ there exists $r \in \mathbb{N}$ with $\Phi_r^\alpha(x_0) \geq \delta$, and for all $m \geq r$,

$$\mathbb{P}(\Phi_m(x_0) \geq \delta) \geq \left(1 - \Phi\left(\frac{\alpha - \omega}{\sigma}\right)\right)^r.$$

where Φ is the standard normal CDF.

Proof. (i) Since $a_{\min} \leq a_j$ for all j and $x_0 > 0$, Lemma A.4 (with $(a_1, \dots, a_m) = (a_{\min}, \dots, a_{\min})$ and $(b_1, \dots, b_m) = (a_1, \dots, a_m)$) implies $\Phi_m(x_0) \geq \phi_{a_{\min}} \circ \dots \circ \phi_{a_{\min}}(x_0)$.

(ii) For $\alpha > \omega > 0$, $\Phi_m^\alpha(x_0)$ is nondecreasing in m and converges to the unique $\xi_\alpha > 0$. Given $0 < \delta < \xi_\alpha$, choose $r \in \mathbb{N}$ such that $\Phi_r^\alpha(x_0) \geq \delta$.

For any $m \geq r$, on the event

$$E_{m,r}(\alpha) := \{a_{m-r+1} \geq \alpha, \dots, a_m \geq \alpha\}$$

Lemma A.4 applied to the last r gains yields $\Phi_m(x_0) \geq \Phi_r^\alpha(\Phi_{m-r}(x_0)) \geq \Phi_r^\alpha(x_0) \geq \delta$, since ϕ is increasing on \mathbb{R}_+ . By independence, $\mathbb{P}(E_{m,r}(\alpha)) = (1 - \Phi((\alpha - \omega)/\sigma))^r$. This proves $\mathbb{P}(\Phi_m(x_0) \geq \delta) \geq (1 - \Phi((\alpha - \omega)/\sigma))^r$. \square

For an integer $\ell \geq 1$ consider the random recursion

$$X_0 := x_0, \quad X_j := f(A_j X_{j-1}) \quad (j = 1, 2, \dots, \ell),$$

where $(A_j)_{j \geq 1}$ are independent and identically distributed as $\mathcal{N}(\omega, \sigma^2)$ for some $\sigma > 0$. Write $\pi_j := \mathbb{P}(X_j < 0)$ for the negative mass at depth j and $p_- := \mathbb{P}(A_1 < 0)$.

Lemma A.5. Let $f \in \mathcal{F}$ and $x_0 > 0$, for every $j \geq 1$,

$$\pi_j = \frac{1}{2} \left(1 - (1 - 2p_-)^j\right), \quad p_- = \mathbb{P}(A_1 < 0) = \Phi\left(-\frac{k}{\sigma}\right). \quad (4)$$

Proof. Since f is odd and strictly increasing, $\text{sign}(f(u)) = \text{sign}(u)$ for all u , hence

$$\{X_j < 0\} = \{A_j X_{j-1} < 0\} = (\{A_j < 0\} \cap \{X_{j-1} > 0\}) \cup (\{A_j > 0\} \cap \{X_{j-1} < 0\}),$$

up to null sets (because $\mathbb{P}(A_j = 0) = 0$ for Gaussian A_j). Independence of A_j and X_{j-1} yields

$$\pi_j = \mathbb{P}(A_j < 0) \mathbb{P}(X_{j-1} > 0) + \mathbb{P}(A_j > 0) \mathbb{P}(X_{j-1} < 0) = p_-(1 - \pi_{j-1}) + (1 - p_-)\pi_{j-1}.$$

Thus $\pi_j = (1 - 2p_-)\pi_{j-1} + p_-$. With $\pi_0 = \mathbb{P}(X_0 < 0) = 0$, the first-order linear recursion solves to

$$\pi_j - \frac{1}{2} = (1 - 2p_-)(\pi_{j-1} - \frac{1}{2}) \implies \pi_j - \frac{1}{2} = (1 - 2p_-)^j (\pi_0 - \frac{1}{2}) = -\frac{1}{2}(1 - 2p_-)^j.$$

The value of p_- follows from $A_1 \sim \mathcal{N}(\omega, \sigma^2)$. \square

Theorem 4.7 Fix a target $p \in [0, \frac{1}{2})$, a depth $\ell \in \mathbb{N}$, and $\omega > 0$. There exists a unique $\sigma^* = \sigma^*(p, \ell, k) > 0$ such that $\pi_\ell(\sigma^*) = p$, and it is given by

$$\sigma^*(p, \ell, k) = - \frac{k}{\Phi^{-1}\left(\frac{1 - (1 - 2p)^{1/\ell}}{2}\right)}. \quad (5)$$

Proof. $\pi_\ell(\cdot)$ is continuous and strictly increasing from 0 (at $\sigma \downarrow 0$) to $1/2$ (as $\sigma \uparrow \infty$). Hence for any $p \in [0, 1/2)$ there exists a unique $\sigma^* > 0$ with $\pi_\ell(\sigma^*) = p$.

To obtain the explicit form, set $q := p_-(\sigma^*) = \Phi(-k/\sigma^*) \in (0, 1/2)$. From Lemma A.5 we have

$$p = \pi_\ell(\sigma^*) = \frac{1}{2} \left(1 - (1 - 2q)^\ell\right) \implies q = \frac{1 - (1 - 2p)^{1/\ell}}{2}.$$

Applying the inverse CDF Φ^{-1} to $q = \Phi(-k/\sigma^*)$ yields

$$-\frac{k}{\sigma^*} = \Phi^{-1}(q) \implies \sigma^* = - \frac{k}{\Phi^{-1}(q)}.$$

Since $q \in (0, 1/2)$, the quantile $\Phi^{-1}(q) < 0$, so the right-hand side is positive. \square

B ADDITIONAL EXPERIMENTAL RESULTS WITHOUT TRAINED NETWORKS

B.1 DEFINITIONS OF ACTIVATION FUNCTIONS

This section introduces the activation functions considered in this paper. The following functions belong to the odd-sigmoid function class.

Gudermannian function The Gudermannian function $\text{gd} : \mathbb{R} \rightarrow \mathbb{R}$ is defined by

$$\text{gd}(x) = \int_0^x \frac{dt}{\cosh t} = 2 \arctan\left(\tanh\left(\frac{x}{2}\right)\right).$$

Error Function. The error function $\text{erf} : \mathbb{R} \rightarrow \mathbb{R}$ is defined as

$$\text{erf}(x) = \frac{2}{\sqrt{\pi}} \int_0^x e^{-t^2} dt.$$

Softsign-Type Functions. For $k \geq 1$, we define the generalized softsign function

$$\text{softsign}_k(x) = \frac{x}{(1 + |x|^k)^{1/k}}, \quad x \in \mathbb{R}.$$

This family interpolates between several commonly used smooth odd activations:

$$\text{softsign}_1(x) = \frac{x}{1 + |x|}, \quad \text{softsign}_2(x) = \frac{x}{\sqrt{1 + x^2}}, \quad \text{softsign}_3(x) = \frac{x}{(1 + |x|^3)^{1/3}}.$$

We also use the combined variant

$$\text{softsign}_{1+3}(x) := \text{softsign}_1(x) + \text{softsign}_3(x).$$

Hyperbolic Tangent. The hyperbolic tangent function $\tanh : \mathbb{R} \rightarrow \mathbb{R}$ is defined by

$$\tanh(x) = \frac{e^x - e^{-x}}{e^x + e^{-x}}.$$

Arctangent. The (scaled) arctangent function $\arctan : \mathbb{R} \rightarrow \mathbb{R}$ is given by

$$\arctan(x) = \int_0^x \frac{dt}{1 + t^2}.$$

In practice, we often use the normalized form $\frac{2}{\pi} \arctan(x)$ so that its range matches that of $\tanh(x)$.

B.2 PROPERTIES OF THE ODD-SIGMOID FUNCTIONS

This section empirically investigates the properties of the iteration $x_{n+1} = f(ax_n)$.

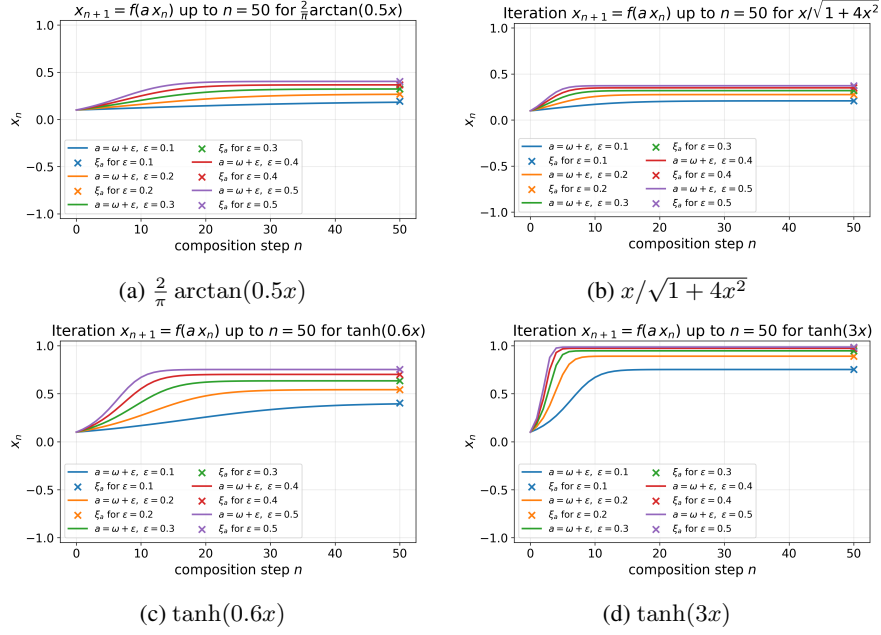


Figure 7: Convergence of the iterates $x_{n+1} = f(ax_n)$ for $f \in \mathcal{F}$ with $a = \omega + \epsilon$ ($\epsilon \in \{0.1, 0.2, 0.3, 0.4, 0.5\}$); curves show x_n up to $n = 50$ from $x_0 = 0.1$, and 'x' marks ξ_a .

B.3 NEGATIVE RATE

This section empirically investigates the relationship among the negative rate p , the calibrated noise scale σ^* , and the dispersion of the last-layer activation distribution (quantified by the entropy-based spread metric).

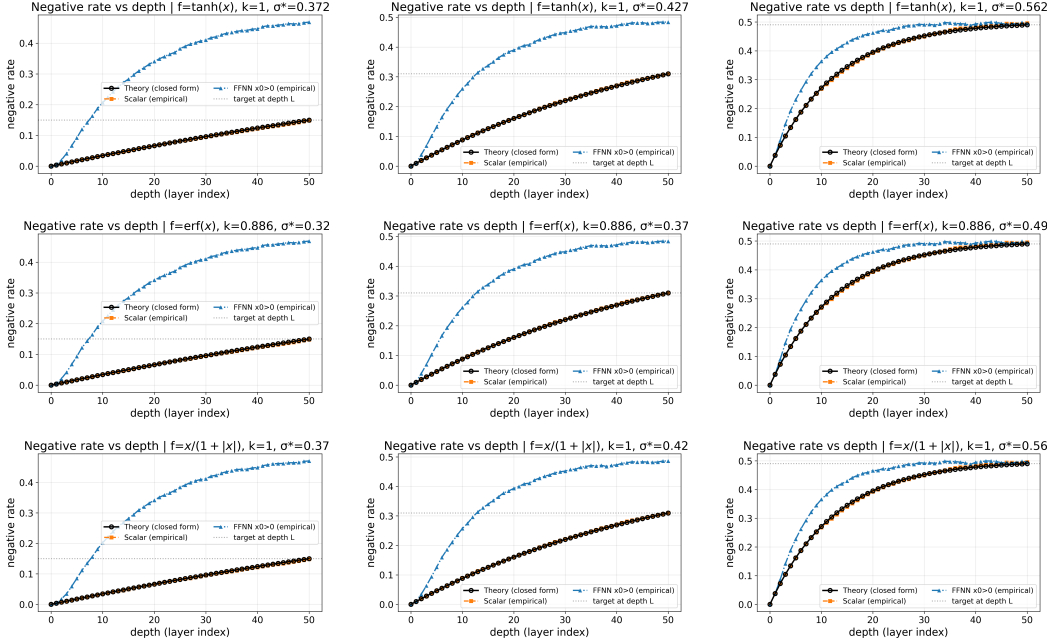


Figure 8: Negative rate versus depth for three odd-sigmoid activations (\tanh , erf , $x/(1+|x|)$) and targets $p \in \{0.14, 0.31, 0.49\}$ at depth 50. In each panel, the noise scale σ^* is set by the closed form in Theorem 4.7 so that $\pi_L(\sigma^*) = p$. Shown are theory (black), a multiplicative scalar chain (orange), and an additive FFNN with $x_0 > 0$ (blue); the dotted line marks p .

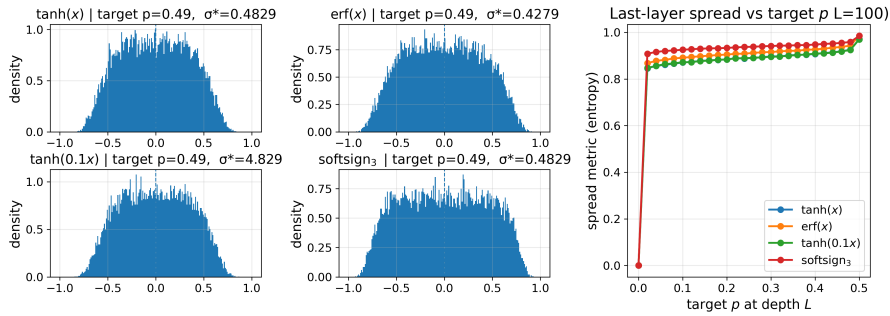


Figure 9: **(Left)** last-layer activation histograms at target $p = 0.49$ for four odd-sigmoid activations (\tanh , erf , $\tanh(0.1x)$, and softsign_3) in a depth-100 feedforward chain (width proxy $n = 20,000$, $x_0 > 0$). For each activation, the noise scale σ^* is set by the closed form $\pi_L(\sigma^*) = p$. **(Right)** last-layer *spread* versus target p (entropy-based metric) under the same setup.

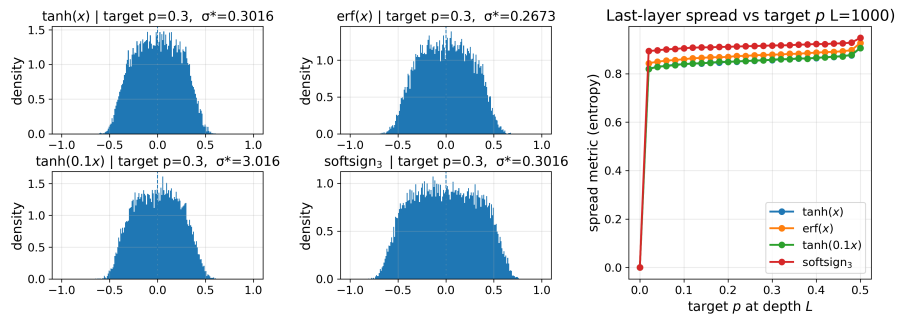


Figure 10: **(Left)** last-layer activation histograms at target $p = 0.3$ for four odd-sigmoid activations (tanh, erf, tanh(0.1x), and softsign₃) in a depth-1,000 feedforward chain (width proxy $n = 20,000$, $x_0 > 0$). For each activation, the noise scale σ^* is set by the closed form $\pi_L(\sigma^*) = p$. **(Right)** last-layer *spread* versus target p (entropy-based metric) under the same setup.

C ADDITIONAL EXPERIMENTAL RESULTS WITH NEURAL NETWORKS

C.1 EARLY EPOCH PERFORMANCE

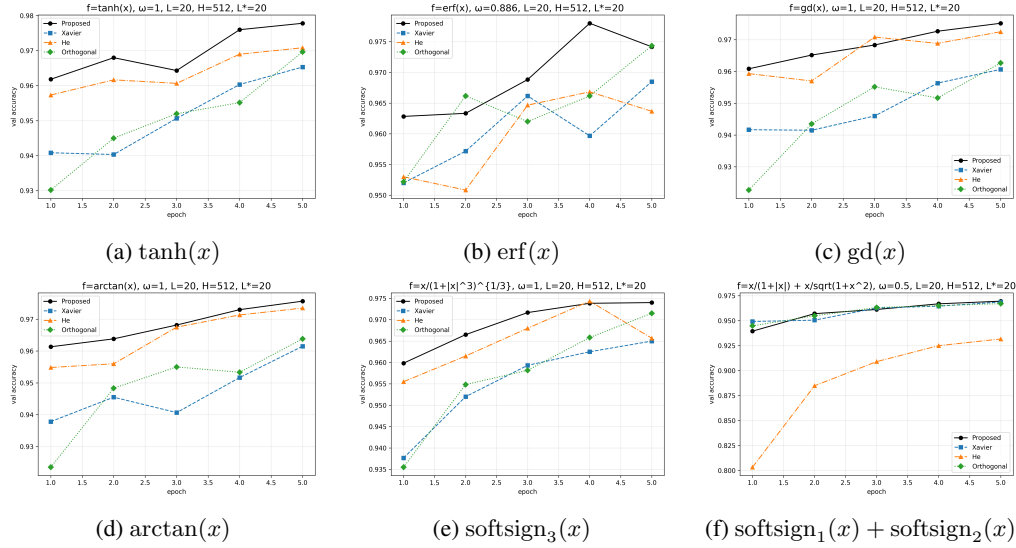


Figure 11: Validation accuracy over 5 epochs for a 20-layer MLP (width 512) on the MNIST dataset, comparing four initializations: Proposed, Xavier, He, and Orthogonal.

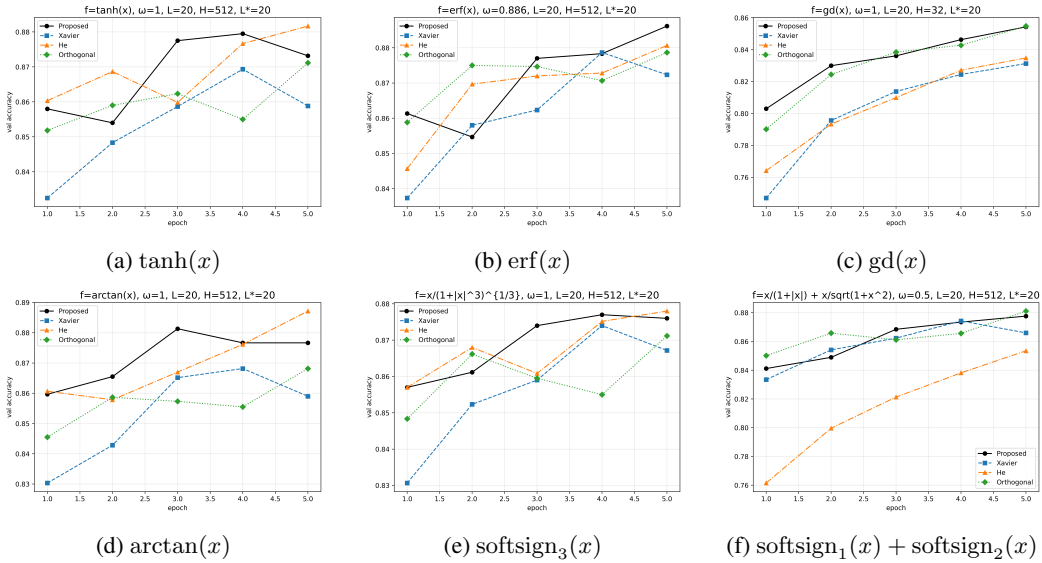


Figure 12: Validation accuracy over 5 epochs for a 20-layer MLP (width 512) on the Fashion MNIST dataset, comparing four initializations: Proposed, Xavier, He, and Orthogonal.

C.2 DATASET EFFICIENCY

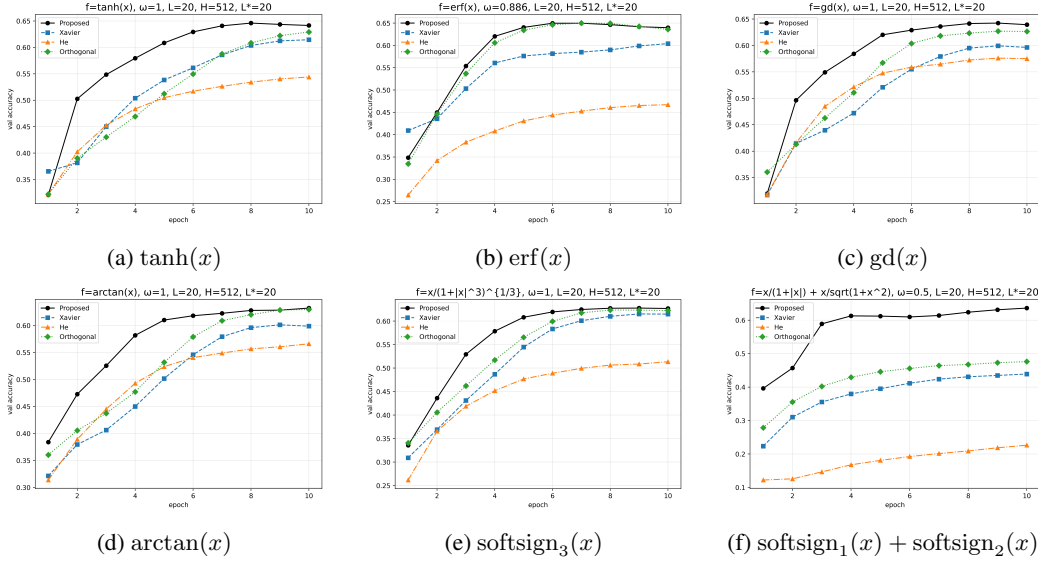


Figure 13: Validation accuracy over 10 epochs for a 20-layer MLP (512 units) on MNIST, trained on a 100-sample subset, comparing four initializations (Proposed, Xavier, He, Orthogonal).

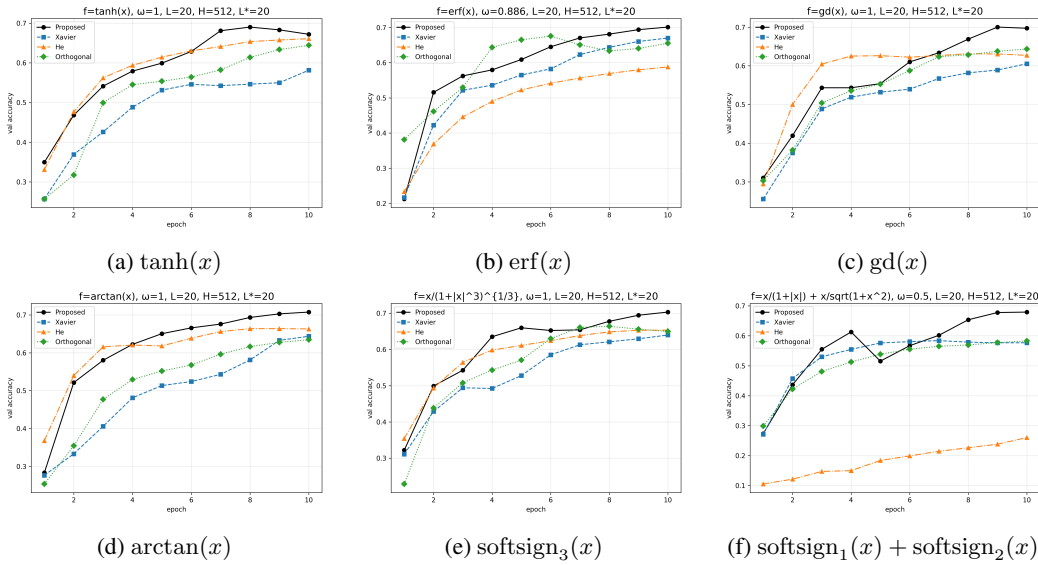


Figure 14: Validation accuracy over 10 epochs for a 20-layer MLP (512 units) on FashionMNIST, trained on a 100-sample subset, comparing four initializations (Proposed, Xavier, He, Orthogonal).

C.3 LEARNABLE LEARNING RATE

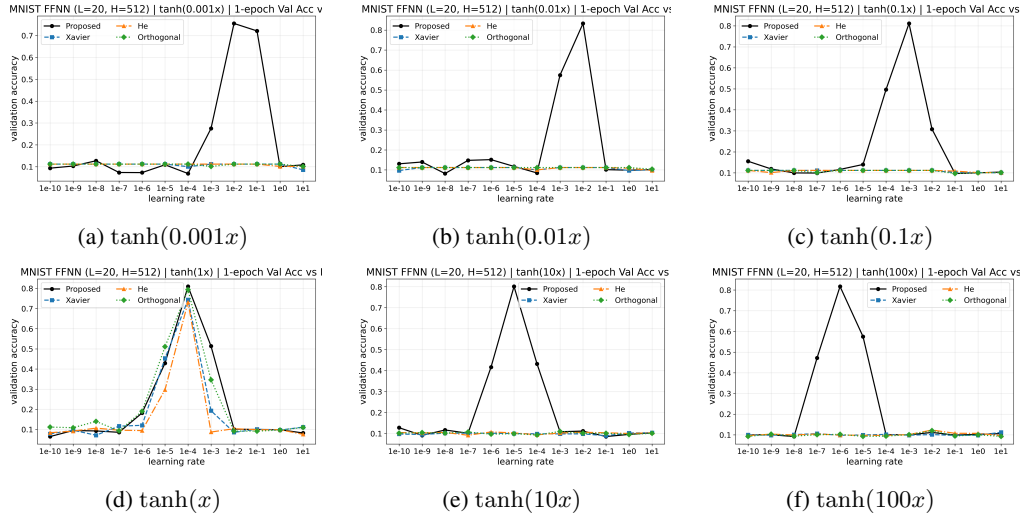


Figure 15: Learnable learning rate ranges activation function over one epoch for a 20-layer MLP (width 512) on MNIST, trained on a 1,000-sample subset. Panels report one-epoch validation accuracy for $f(x) = \tanh(\alpha x)$ with $\alpha \in \{10^{-3}, 10^{-2}, 10^{-1}, 1, 10, 100\}$ across four initializations (Proposed, Xavier, He, Orthogonal).

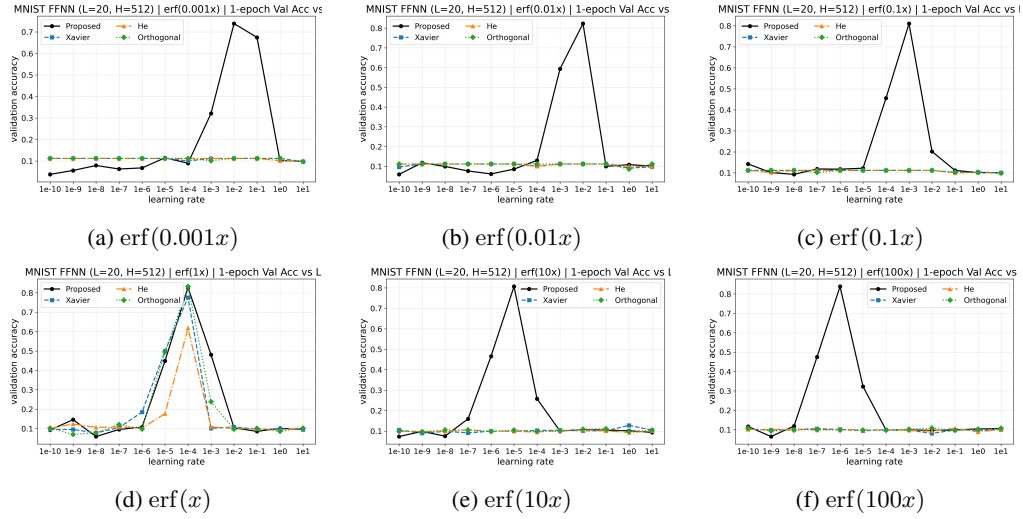


Figure 16: Learnable learning rate ranges activation function over one epoch for a 20-layer MLP (width 512) on MNIST, trained on a 1,000-sample subset. Panels report one-epoch validation accuracy for $f(x) = \text{erf}(\alpha x)$ with $\alpha \in \{10^{-3}, 10^{-2}, 10^{-1}, 1, 10, 100\}$ across four initializations (Proposed, Xavier, He, Orthogonal).